NANO LETTERS

2006
Vol. 6, No. 1
66−72

Autonomously Moving Nanorods at a Viscous Interface

P. Dhar,[†] Th. M. Fischer,*,[†] Y. Wang,[‡] T. E. Mallouk,[‡] W. F. Paxton,[‡] and A. Sen[‡]

Department of Chemistry and Biochemistry, The Florida State University, Tallahassee, Florida 32306-4390, and Department of Chemistry, The Pennsylvania State University, University Park, Pennsylvania 16802

Received October 12, 2005; Revised Manuscript Received November 22, 2005

ABSTRACT

We study the autonomous motion of catalytic nanorods in Gibbs monolayers. The catalytic activity of the rods on a hydrogen peroxide aqueous subphase gives rise to anomalous translational and rotational diffusion. The rods perform a Levy-walk superdiffusive motion that can be decomposed into thermal orientation fluctuations and an active motion of the rods with a constant velocity along their long axis. Since interfacial dissipation increases relative to bulk phase dissipation when miniaturizing the size of objects moving in the interface, the autonomous nanorods allow for precise measurements of surface shear viscosities as low as a few nN s/m. The cross over from active motion toward passive diffusion when increasing the surfactant concentration is explained by a loss of friction asymmetry of the rods.

The new frontier for the experimental study of soft condensed matter systems targets behavior under nonequilibrium conditions. In a fluid system, molecules, such as surfactants and block copolymers, or larger structures such as colloids[1,2] are free to flow around and assemble themselves into new nanoscale materials. Active components are either components that autonomously move in the hydrodynamic assembly or components that start to move due to the application of a dynamic electric or magnetic field. Our understanding of the structure and fluctuations of passive complex fluids at thermal equilibrium has significantly increased over the past decades. However, scientists are just beginning to understand dynamic complex fluids containing active nanocomponents that consume energy and play an important role in the maintenance of stationary nonequilibrium patterns. In this work we study active nanocomponents near interfaces. Active components give rise to emergent phenomena such as dynamic self-assembly[3−5] and anomalous fluctuations[6,7] and diffusion.[8−10] Realistic models for the dynamic behavior of the biological cell and for hydrodynamics of lab-on-a-chip devices[11] have to account for these nonequilibrium properties. The first step in understanding dynamic complex fluids is the design of the active components. Their size varies from single proteins,[7] over nanomotors[12,13] to the millimeter scale.[3,4] Active components can translate[12,13] and rotate[3−5,14] in their environment. In nanometer-sized systems the flow is dominated by the hydrodynamic boundary conditions at either the liquid/solid or liquid/air interface or even the three-phase intersection line. It is therefore clear that understanding the energetics, interfacial hydrodynamics,[15] and interactions of active nanocomponents is one of the keys for an optimized design of a hydrodynamic nanodevice.

The current work uses active nanocomponents to study their interaction with the surroundings and their energy consumption. At the liquid/liquid interface our model system is a composite mixture of surfactants forming a monolayer and self-propelling nanorods that are bound to the interface by capillary forces. The nanorods catalyze a chemical reaction in the subphase and move in the monolayer surroundings.

Gibbs monolayers are assemblies of soluble surfactants at the liquid/liquid interface that can alter the hydrodynamic behavior of the interfaces. The rheological properties of the liquid/liquid interface can be widely tuned via the surface density of surfactants that is easily controlled by the bulk concentration that is in thermodynamic equilibrium with the surface. In very dense monolayers with proteins incorporated into the interface, the typical surface shear viscosity can be of the order of 10^{-5} N s/m and higher, while in a liquid phase it is at least 6 orders of magnitude lower. If the viscosity is high, one usually encounters viscoelastic behavior of the interface,[16−21] while for small viscosities the surface can be considered to be only viscous.[22−30] Indeed in liquid phases the value of the viscosity is so low that it has not been possible to measure.[28−30] The use of autonomous nanomotors moving within the interface here is to measure the rheological behavior of liquid/liquid interfaces and their effect on the nanomotors in a regime that has not been able to be measured with other techniques.

[†] The Florida State University.
[‡] The Pennsylvania State University.

10.1021/nl052027s CCC: $33.50
Published on Web 12/14/2005

The analysis of the motion of objects at interfaces in which the surface viscosity dominates has been pioneered by Saffman and Delbrück[31] who realized that on a small scale the theoretical treatment of the surface flow may be approximated by treating the surface as incompressible. Such an approximation is equivalent to an instantaneous response of the surface to perturbations in surface density of surfactants, which holds if shear rates are low in comparison to the equilibration rate of surface density waves. The presence of nanomotors at the interface perturbs the hydrodynamics of the inactive monolayer. One might think that the hydrodynamic behavior of motors at interfaces might behave similar to what one observes for motors in a three-dimensional fluid. This, however, is not the case. Saffman and Delbrück[31] also showed that the ratio between the two-dimensional (2d) viscosity[32] of the membrane and three-dimensional (3d) viscosity of the bulk phase defines a length scale, the *Boussinesq length* l_B, that is characteristic for the coupled membrane/bulk phase system. The mobility of objects within a membrane depends strongly on whether the size of the motor is smaller than l_B or larger than l_B. Nanomotors in membranes move according to hydrodynamic rules that are significantly different from the rules for macroscopic motors at interfaces. Many biomembranes that appear homogeneous on a macroscopic scale are heterogeneous on the nanoscale. Heterogeneities in the interface on length scales below l_B lead to hydrodynamic behavior that is a complex mixture of 2d and 3d hydrodynamic interactions.

Saffman and Delbrück's[31] work was later extended to the bulk flow dominated case[33] and to different geometries such as thin water layers[24] and protruding spherical particles.[34,35] The geometries of interest here is that of thin rods of high aspect ratio moving in the interface.[36] Catalytic nanomotors based on asymmetric platinum−gold nanorods (diameter 370 nm length 1 + 1 μm) autonomously move[12] in a mixture of hydrogen peroxide and water. The platinum catalyses the decomposition of the peroxide into water and oxygen and the rods are propelled in the direction of the platinum end by the oxygen concentration gradient[13] and the asymmetry of the rod (Figure 1). The chemical power produced by one H_2O_2 molecule reacting every 10 s (Gibbs free energy of reaction, $\Delta G \approx -50\ k_BT$ per molecule of H_2O_2) is enough to account for the mechanical propulsion power. In reality there are many more molecules reacting at the rod per unit time ($\dot{N}_{H_2O_2} \approx 10^9\ s^{-1}$), and we find that only a minute fraction of the Gibbs free energy of reaction is actually spent on propelling the rod through the liquid.

The platinum gold nanorods were prepared as described in ref 12. To spread them on a 4% hydrogen peroxide aqueous solution, they were dialyzed in methanol and then spread on the air−water surface that was covered with decane after the deposition of the rods. We varied the rheological properties of $H_2O_{2(aq)}$/decane interface by dissolving sodium dodecyl sulfate (SDS) in the aqueous solution at concentrations 0−10 mM. The critical micelle concentration (cmc) of SDS is cmc = 0.8 mM. The SDS forms a Gibbs monolayer at the interface that is in thermodynamic equi-

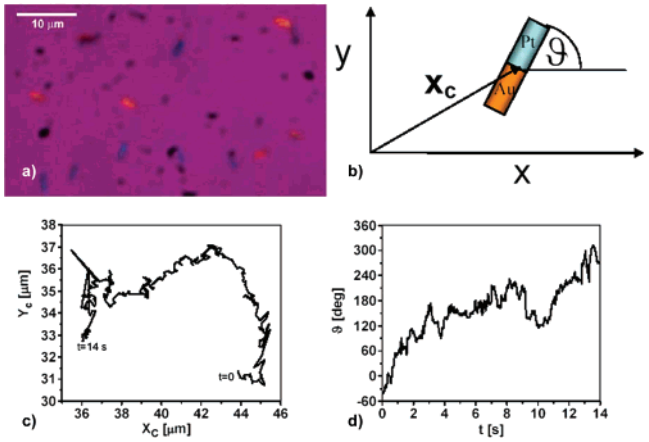

Figure 1. (a) Polarization microscope image (crossed polarizers with a λ plate) of a collection of nanorods at the aqueous hydrogen peroxide solution/decane interface. The rods appear in different colors depending on their orientation. (b) Schematic defining the center of mass $\mathbf{x}_c$ and orientation ϑ of the rod. (c) Levy-walk type trajectory of a rod on a bare (no SDS) $H_2O_{2(aqu)}$/decane interface. (d) Orientation fluctuations of the same rod on a bare $H_2O_{2(aqu)}$/decane interface.

librium with the bulk concentration. We then follow the kinetics of individual nanorods. Each nanorod is described by its center of mass $\mathbf{x}_c(t)$ and by its orientation that we characterize with the angle $\vartheta(t)$ between its long axis oriented toward the platinum end and some arbitraty chosen axis fixed in the laboratory system; see Figure 1b. Movies of the rod motion observed with a microscope are taken and digitized, and $\mathbf{x}_c(t)$ and $\vartheta(t)$ values are extracted for each frame of the digitized movie. Figure 1c shows a typical trajectory of the center of mass and Figure 1d depicts the angular fluctuation of the same rod on the bare decane−water interface as a function of time. The trajectory of the rod is much more open structure than that which is observed from Brownian motion, and it is caused by the active motion of the rod. It is a fractal structure like those found in a Levy-walk superdiffusive processes.[37] Levy-walk diffusion is characterized by a correlation function

$$C(\tau) := \langle (\mathbf{x}_c(t) - \mathbf{x}_c(t+\tau))^2 \rangle \propto \tau^{\alpha} \qquad (1)$$

with an exponent $1 < \alpha < 2$. Here the brackets $\langle A \rangle = (1/T) \int_0^T dt\ A(t)$ denote the time average.

Figure 2 displays a double logarithmic plot of $C(\tau)$ calculated from the raw data $\mathbf{x}_c(t)$ for rods placed on $H_2O_{2(aqu)}$/decane interfaces of varying SDS content.

The plot shows that at low SDS concentrations the rods move away from their initial position following a power law $C(\tau) = 4D\tau^{\alpha}$ with an exponent $\alpha = 1.6 \pm 0.1$ that is typical for a Levy-walk type of diffusion. A Levy walk is a random walk with frequent long periods where the particles move in one direction with a defined velocity. The superdiffusive Levy-walk coefficient D is largest for the bare decane−water interface and decreases when adding a very low amount of surfactant to the interface. The exponent drops to $\alpha = 1 \pm 0.1$ at high SDS concentration which corresponds to a normal

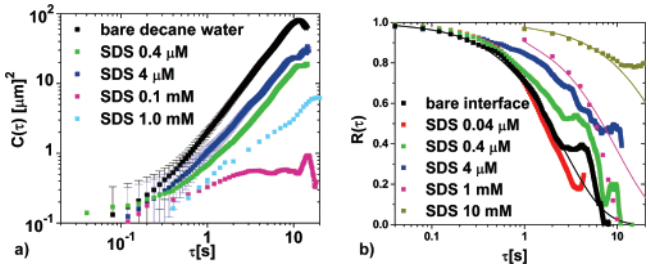

Figure 2. (a) Plot of the correlation function $C(\tau)$ versus time accumulated over a period $T \approx 10\gamma^{-1}$ ($T = 14$ s for the bare air−water surface, $T = 140$ s for the 10 mM SDS solution) by following a single rod. The error bars (0.2 μm^2) reflect the accuracy (400 nm) in the determination of $\mathbf{x}_c$. (b) Plot of the angular correlation function $R(\tau)$ of the rods on a $H_2O_{2(aqu)}$/decane interface for various subphase concentrations of SDS. The lines are fits according $R(\tau) = e^{-\gamma\tau}$. The experimental curves deviate from the theory at large τ due to lack of statistics because of a finite accumulation time T. The relative statistical error from the finite accumulation time T is of the order τ/T and not depicted in the figure.

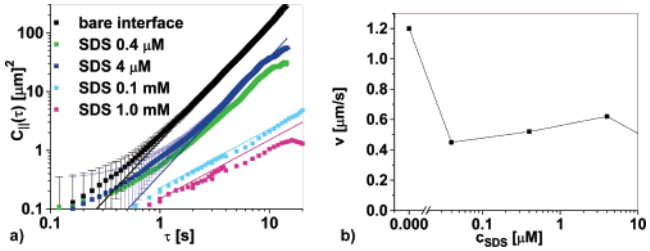

Figure 3. (a) Correlation function of the rod motion parallel to its long axis for various SDS subphase concentrations calculated from the same raw data as in Figure 2. The correlation functions follow the law $C_{||}(\tau) = v^2\tau^2$ (black and blue lines) at low SDS concentration and a diffusive behavior $C_{||}(\tau) = 2D_{||}\tau$ (cyan and magenta line) at high SDS concentration. The velocity v is shown as a function of the SDS concentration in (b) for $c_{SDS} < 10$ μM.

diffusive motion. In Figure 2b we plot the correlation function $R(\tau) := \langle\cos(\vartheta(t) - \vartheta(t+\tau))\rangle$. The angular correlation follows an exponential decay $R(\tau) = e^{-\gamma\tau}$ with a rotational diffusion constant γ that decreases with increasing SDS concentration. The orientation correlation function $R(\tau)$ does not depend on the amount of H_2O_2 dissolved in the aqueous phase. It looks the same with and without H_2O_2 (not shown). The Levy-walk superdiffusion of the center of mass can be understood by the superposition of the thermal orientational fluctuations of the rod and a movement at constant speed v in the direction of the momentary platinum end direction that is caused by the reaction of H_2O_2. To see this, we define the **c**-director as $\mathbf{c} = (\cos\vartheta, \sin\vartheta)$. The velocity of the rod is given by the time derivative of the center of mass $\mathbf{v} = \dot{\mathbf{x}}_c$. The length $s_{||}(t)$ the rod is propelled in direction of the platinum end after time t is then given by $s_{||}(t) = \int_0^t \mathbf{c}(t')\cdot\mathbf{v}(t')\,dt'$ while the length the rod moved in the direction of its short axis is $s_\perp(t) = \mathbf{e}_z\cdot\int_0^t \mathbf{c}(t')\times\mathbf{v}(t')\,dt'$ with $\mathbf{e}_z$ the unit vector perpendicular to the interface. We then define the correlation functions of the motion parallel and perpendicular to the rod as $C_{||}(\tau) = \langle(s_{||}(t) - s_{||}(t+\tau))^2\rangle$ and $C_\perp(\tau) = \langle(s_\perp(t) - s_\perp(t+\tau))^2\rangle$. Computation of both correlation functions from the raw data $\mathbf{x}_c(t)$ and $\vartheta(t)$ reveals that $C_\perp(\tau) \ll C_{||}(\tau)$ and there is hardly any motion perpendicular to the rod. Figure 3a shows $C_{||}(\tau)$ for various SDS concentrations. We again find a power law behavior for $C_{||}(\tau)$ for both low and high SDS concentration but now with a low SDS concentration exponent $\alpha_{||} = 2 \pm 0.1$ that is a motion with constant velocity v according to $C_{||}(\tau) = v^2\tau^2$. The speed v of the rods is depicted in Figure 3b as a function of the SDS subphase concentration. At higher SDS concentrations $c_{SDS} > 0.1$ mM the exponent drops to $\alpha_{||} = 1 \pm 0.1$, which corresponds to normal edge on diffusion of the rods $C_{||}(\tau) = 2D_{||}\tau$, with $D_{||}$ the diffusion constant for diffusion along the long axis of the rod.

Rotational Motion. To understand the origin of the rotational motion, we need to calculate the viscous torque on a rotating rod. The torque T on a solid rod of length l and diameter d rotating with angular frequency ω in a bulk fluid of viscosity η was calculated first by Burgers[38]

$$T = \frac{\pi}{3}\frac{\eta l^3\omega}{\ln(2l/d) - 0.8} \tag{2}$$

At the interface, half of this bulk torque is exerted to the subphase and the other half to the superphase. However, additional torque arises due to Marangoni forces and surface viscous forces. We approximate the total torque as a sum of the bulk and surface contributions

$$T = (f_b + f_s)(\eta_1 + \eta_2)l^3\omega \tag{3}$$

where

$$f_b = \frac{\pi}{6(\ln(2l/d) - 0.8)} \tag{4}$$

is the bulk contribution to the torque according to Burgers[38] and f_s the surface contribution, η_1 and η_2 are the bulk viscosities of the sub- and superphases. The surface contribution $f_s(B)$ depends on the Boussinesq number

$$B = \eta_s/(\eta_1 + \eta_2)l \tag{5}$$

with η_s the surface shear viscosity. We calculated this contribution in the limit of vanishing rod radius (Appendix). The result is depicted in Figure 4. The asymptotic value for $B \to 0$ describes the Marangoni contribution to the torque, while the value for $B \to \infty$ amounts for the surface viscous contribution.

We fit the rotational diffusion constant γ to the experimentally measured angular correlation function as $R(\tau) = e^{-\gamma\tau}$. From the Stokes Einstein relation we conclude that

$$f_s(B) = \frac{k_B T}{(\eta_1 + \eta_2)l^3\gamma} - f_b \tag{6}$$

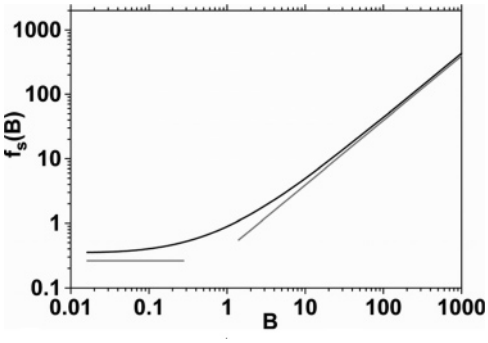

Figure 4. Surface torque coefficient $f_s(B)$ as a function of the Boussinesq number. The gray lines are the asymptotic relations given in eq A7.

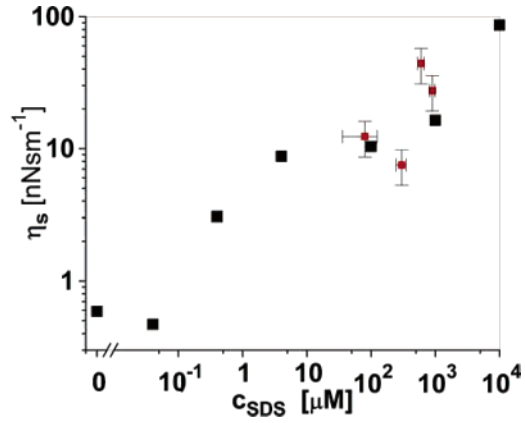

Figure 5. Surface shear viscosity of the decane/water interface (black) as determined from the angular correlation function $R(\tau)$ of the rod orientation. The red data points are the viscosity of SDS in a stearic acid monolayer at the air/water interface as measured by Khattari et al.[40]

From our numerical results in Figure 4 we convert the surface torque coefficient $f_s(B)$ into a Boussinesq number. The surface shear viscosity of the interface is then obtained via eq 5. Figure 5 shows the surface shear viscosity of the decane/water interface as a function of the SDS concentration.

The surface shear viscosity calculated in Figure 5 agrees with data from Bouchama and di Meglio[39] and of Khattari et al.[40] The independence of $R(\tau)$ from the H_2O_2 concentration and the agreement of the surface shear viscosity data with other measurements show that the orientation fluctuations are of thermal origin. Note that the orientation fluctuations of the nanorods do not require a particular boundary condition for the parallel component of the velocity, since there is only a normal component on the surface of the rod. Chemophoretic flow,[13] such as that induced by the catalytic reaction of H_2O_2, leads to an apparent slip velocity[41] at the boundary of the rod of the parallel component of the velocity. For spherical bodies this boundary condition couples to a chemophoretic rotation of the object. For long rotating rods, however, a parallel component of the velocity may only occur at the ends of the rod that expose negligible area to the adjacent fluid. It is for this reason that chemophoretic motion only couples to the translational motion along the long axis of the rod.

Translational Motion. The translational motion crosses over from a H_2O_2 propelled motion toward a thermal diffusion. Typical speeds of the rods on a bare $H_2O_{2(aqu)}$/decane interface are of the order $v \approx 1$ μm/s, and the dissipated energy necessary to propel the rod by a distance equal to its length with this speed is on the order of k_BT. The system therefore is not far away from equilibrium. In ref 12 the chemophoretic motion of the rods could be estimated by solving the convection diffusion equation for the oxygen produced; however, the direction of the motion could not be explained. One hypothesis is that the direction of the motion of the nanorods is caused by a hydrodynamic friction asymmetry and that the rod will move in the direction where the friction is minimal. If the rod moves in direction of the platinum end, the oxygen produced at the platinum surface will be advected toward the gold end of the rod. There the oxygen lubrication will significantly decrease the viscous drag on the moving rod as the viscosity of oxygen is a factor 10^{-3} smaller than that of the hydrogen peroxide solution. If the rod were moving in the opposite direction, the oxygen produced near the platinum surface would not pass the gold surface and hence would not lubricate the rod. The viscous friction of the motion in the direction of the platinum end is therefore smaller than that for the motion in the opposite direction. Whatever mechanism is responsible for the propulsion of the rod, the chemical reaction is catalyzed by the platinum section of the rod resulting on average in a symmetric arrangement of both products and reactants around the platinum section. Fluctuations around this symmetric arrangement then create a concentration gradient in an arbitrary direction. The motion, however, generated by these fluctuations is not symmetric around the rod due to the asymmetric friction, and the rod exhibits a mean velocity in the direction of the Pt. Our hypothesis of the rod motion is similar to that of a thermal ratchet, with the thermal noise being replaced by the chemical noise and the asymmetric potential by an asymmetric friction.

The experiments of the motion of the rods in the SDS-covered $H_2O_{2(aqu)}$/decane interface support this hypothesis. The translational drag for edge on motion of the rod has been calculated by Fischer.[36] The translational diffusion constant is given by $D_{||} = k_BT/(\eta_1 + \eta_2)lf_{II}(B)$, where the dimensionless friction constant f_{II} is taken from ref 36. We insert the Boussinesq number obtained from the rotational motion into the translational motion and fit the translational correlation function with a diffusive motion: $C_{||} = 2D_{||}\tau$. Such fitting gives reasonable agreement if the Boussinesq number is larger than 1, i.e., if $c_{SDS} > 0.1$ mM (see Figure 3). This proves that the translational motion reduces to thermal Brownian motion if the Boussinesq length is larger than the length of the rod.

The flow profile around the rod as calculated in ref 36 distinguishes a region closer than l_B and farther than l_B from the rod. In the closer region the velocity varies approximately logarithmic with the distance from the rod, while further away it rapidly changes inversely proportional to the distance. Neglecting the weak logarithmic decay, one could say, in a simplified way, that the surface viscosity has the effect of

increasing the hydrodynamic radius of the rod by l_B. Hence the rod in the viscous interface moves as if a larger object would be moving in a nonviscous interface. We hence can think of the rod plus a region of l_B as a solid object. The effect of the region of size l_B is to render the asymmetric platinum gold rod hydrodynamically more symmetric. Oxygen produced near the platinum surface can lubricate the relatively rigid region of size l_B surrounding the rod no matter in which direction the rod decides to move. Hence, if l_B is larger than the length of the gold section of the rod, the friction of the moving rod is more symmetric and there is no longer any preferential direction of motion of the rod. The surface viscosity will quench both the thermal diffusive and the H_2O_2 propelled motion; however, due to the friction now being symmetric, the quenching of the mean propulsion speed is more pronounced than the quenching of the thermal motion. The ratio of the strength of the active versus the thermal diffusion is changed and now diffusion is stronger than active motion, which we observe as a cross over of the exponent $\alpha_{||}$ of the correlation function $C_{||}$.

The assumption of an on average symmetric concentration profile holds if the gold section is not involved in the chemical reaction. However, the concentration profile might be rendered asymmetric for electrochemical reasons. The electromotoric force $E_{Au/Pt} = 0.49$ V between gold and platinum generates an electric field with an asymmetric H^+ concentration profile that could be also the cause of the motion direction.[42] If the SDS affects the catalytic activity of the platinum (e.g., by poisoning the surface or making it less accessible; in ref 12 it is shown that the rate of oxygen production is decreased by the addition of ethanol), then one would expect that the surfactant will quench the directed motion more strongly than simple Brownian motion. In this explanation, however, the location of the crossover in the regime where l_B exceeds the length of the gold section of the rod is a mere accidental coincidence.

Design of Faster Nanorods. In this section we discuss the design of nanorods resulting in higher speeds. From what was said previously it is clear that the asymmetry of the rod is most important for optimal conversion of Gibbs free energy of reaction into rod propulsion. Rods of different lengths and different ratios of Pt:Au were fabricated. In one series, the length of the Pt segment was constant (1 μm), the lengths of the gold segments were 0, 1, 3, or 4 μm, and the speeds of the rods in bulk 3.3% H_2O_2 were measured using a manual particle tracking program (PhysVis from Kenyon College) (Table 1). As one can see the velocity of the rods is fastest for those rods with a 1:1 length ratio corresponding to maximum asymmetry. The finite velocity of the pure platinum rods is due to residual asymmetry in the geometry of the rods that occurs in the production procedure. In addition, rods of varying lengths with a 1:1 ratio of Pt to Au lengths were also fabricated. The speed of these rods in 3.7% H_2O_2 was measured using an automated particle tracking program written by Paul T. Baker: The speed of the rods increases as one miniaturizes the rods. This is reasonable as one expects the friction to scale with the rod length and fluctuations in force to also increase with decreasing rod size. Further down scaling of the rod size will therefore be the pathway to make the objects more efficient movers.

Table 1. Rod Forward Speed of Platinum Rods of Different Design

(a) rods of different length ratio				(b) rods of different total length with optimal 1:1 length ratio		
L_{Pt} (μm)	L_{Au} (μm)	v (μm/s)	n	L_{rod} (μm)	v (μm/s)	n
0.75−1.5	0	2.65	12	2	6.59	10
1	1	6.59	68	4	2.70	87
1	3	1.48	20	6	2.36	47
1	4	1.41	8	8	0.98	64

Conclusions. Platinum gold nanorods at an $H_2O_{2(aqu)}$/decane interface exhibit thermal orientation fluctuations that slow as one adds a soluble surfactant. The orientational fluctuations can be used to measure the surface shear viscosity of the Gibbs monolayer forming at the interface as a function of the subphase concentration. The translational motion along the long axis of the rod is in agreement with thermal diffusion along the rod if the Boussinesq length exceeds the length of the rod. If the rod length is longer than the Boussinesq length, the rods are propelled with a constant velocity in the direction of the platinum end. The motion is generated by the catalytic decomposition of the hydrogen peroxide to water and oxygen. Our measurements support either an electrochemical origin of the motion direction or the hypothesis that the reaction of H_2O_2 creates fluctuating forces. The force fluctuations lead to a mean velocity of the rod in the direction of the platinum end because lubrication of the inert gold section of the rod when the gold is lying downstream leads to an asymmetry of the hydrodynamic friction. Coating the rod with a *rigid* surfactant layer of the size of the Boussinesq length restores the symmetry of the friction when the Boussinesq length exceeds the length of the rod. Consequently the active motion crosses over to a diffusive motion. The combination of orientation fluctuation with the translational motion of the rods along their long axis gives rise to Levy-walk superdiffusive motion. Nanorods should have a length ratio of 1:1 of the platinum and gold section and should be further be miniaturized for most effective motion performance.

Acknowledgment. We thank Paul T. Baker for developing the rod tracking program. Financial support from the Penn State Center for Nanoscale Science and NSF-MRSEC, DMR-021362, is highly acknowledged.

Appendix

In this appendix we outline the calculation of the surface contribution to the torque on the rotating rod. We calculate the surface torque onto the rod arising from Marangoni and surface viscous effects in the limit of vanishing diameter. This torque is defined from the integral equation

$$\mathbf{u}_s(\mathbf{x}) = \int_P \mathbf{O}(\mathbf{x} - \mathbf{x}')\cdot\tau(\mathbf{x}') \tag{A1}$$

that relates the force density $\tau(\mathbf{x}')$ acting on the rod at its perimeter P to the surface velocity profile $\mathbf{u}_s(\mathbf{x})$. $\mathbf{O}(\mathbf{x} - \mathbf{x}')$ is the Oseen tensor, which is a point force solution to the Stokes equation of the monolayer that is coupled to the subphase. Its transverse component reads[36]

$$O_{||}(r) = \frac{1}{4(\eta_1 + \eta_2)} \frac{\mathrm{d}}{\mathrm{d}r}\left[\mathbf{H}_1\left(\frac{r}{Bl}\right) - N_1\left(\frac{r}{Bl}\right) - \frac{2}{\pi}\frac{Bl}{r}\right] \tag{A2}$$

where r is the distance between the location of the force and the location of the velocity, $B = \eta_s/(\eta_1 + \eta_2)l$ is Boussinesq's number, η_s is the surface shear viscosity, and l is the rod length. $\mathbf{H}_1$ denotes the Struve function of the order 1 and N_1 is a Bessel function of the second kind and order 1. We set the x coordinate in the interface perpendicular to the rod and the y coordinate is parallel to the rod. The distance r between the force excerted from the rod at one location and the resulting velocity of the fluid at another location on the rod is then given simply by $r = |y - y'|$. The requirement that the rod should rotate with angular velocity leads to the condition

$$\mathbf{u}_s(y) = \omega y \mathbf{e}_x \quad \text{for} \quad -l/2 < y < l/2 \tag{A3}$$

Equations A2 and A3 define an integral equation for the force density $\tau(y)$. The Oseen tensor simplifies in the limit $B \to 0$ and $B \to \infty$. We find

$$\lim_{B\to 0} O_{||}(|y - y'|) = \frac{1}{(\eta_1 + \eta_2)\pi}\,\delta(y - y') \tag{A4}$$

$$\lim_{B\to\infty} O_{||}(|y - y'|) = \frac{1}{4(\eta_1 + \eta_2)\pi Bl}\left[\ln\frac{|y - y'|}{2Bl} + \gamma + \frac{1}{2}\right]$$

where $\delta(y - y')$ is Dirac's delta function and $\gamma = 0.5772$ is Euler's number. The analytical solutions to the force profile in these limits are

$$\lim_{B\to 0} \tau(y') = \frac{12T_s}{l^2}\frac{y'}{l} \tag{A5}$$

$$\lim_{B\to\infty} \tau(y') = \frac{8T_s}{\pi l^2}\frac{y'}{\sqrt{l^2/4 - y'^2}}$$

where $T_s = \int_{-l/2}^{l/2} \mathrm{d}y' y' \tau(y')$ is the torque from the surface on the rod. The torque from the surface on the rod is proportional to the angular velocity and may be expressed as

$$T_s = (\eta_1 + \eta_2)\omega l^3 f_s(B) \tag{A6}$$

where $f_s(B)$ is the dimensionless friction coefficient. Inserting the solutions (A5) into (A1) with the asymptotic Oseen tensors (A4) and comparison with the left-hand side of the equation then yields

$$\lim_{B\to 0} f_s(B) = \frac{\pi}{12} \tag{A7}$$

$$\lim_{B\to\infty} f_s(B) = \frac{\pi}{4}B$$

The dimensionless torque coefficient $f_s(B)$ as a function of the Boussinesq number over the whole range of Boussinesq numbers is calculated by numerically inverting eq A1. The results of this inversion are depicted in Figure 4.

References

(1) Happel, J.; Brenner, H. *Low Reynolds number hydrodynamics*; Martinus Nijhoff Publishers: The Hague/Boston/Lancaster, 1983.
(2) Russel, W. B.; Saville, D. A.; Schowalter, W. R. *Colloidal dispersions*; Cambridge Monographs on mechanics and applied mathematics; Cambridge University Press: Cambridge, 1989.
(3) Grzybowski, B. A.; Stone, H. A.; Whitesides, G. M. Dynamic self-assembly of magnetized, millimetre-sized objects rotating at a liquid−air interface. *Nature* **2000**, *405*, 1033−1036.
(4) Grzybowski, B. A.; Whitesides, G. M. Three-dimensional dynamic self-assembly of spinning magnetic disks: Vortex crystals. *J. Phys Chem. B* **2002**, *106*, 1188−1194.
(5) Lenz, P.; Joanny, J. F.; Jülicher, F.; Prost, J. Membranes with rotating motors. *Phys. Rev. Lett.* **2003**, *91*, 108104, 1−4.
(6) Ramaswamy, S.; Toner, J.; Prost, J. Nonequilibrium Fluctuations, Traveling Waves, and Instabilities in Active Membranes. *Phys. Rev. Lett.* **2000**, *84*, 3494−3497.
(7) Girard, P.; Prost, J.; Bassereau, P. Passive or Active Fluctuations in Membranes Containing Proteins. *Phys. Rev. Lett.* **2005**, *94*, 088102, 1−4.
(8) Wu, X. L.; Libchaber, A. Particle Diffusion in a Quasi-Two-Dimensional Bacterial Bath. *Phys. Rev. Lett.* **2000**, *84*, 3017−3020.
(9) Kim, M. J.; Breuer, K. S. Enhanced diffusion due to motile bacteria. *Phys. Fluids* **2004**, *16*, L78−L81.
(10) Darnton, N.; Turner, L.; Breuer, K.; Berg, H. C. Moving fluid with bacterial carpets. *Biophys. J.* **2004**, *86*, 1863−1870.
(11) Stone, H. A.; Stroock, A. D.; Ajdari, A. Engineering flows in small devices Microfluidics Toward a Lab-on-a-Chip. *Annu. Rev. Fluid Mech.* **2004**, *36*, 381−411.
(12) Paxton, W. F.; Kistler, K. C.; Olmeda, C. C.; Sen, A.;. St. Angelo, S. K.; Cao, Y.; Mallouk, T. E.; Lammert, P. E.; Crespi, V. H. Catalytic Nano-motors: Autonomous Movement of Striped Nanorods. *J. Am. Chem. Soc.* **2004**, *126*, 13424−13431.
(13) Golestanian, R.; Liverpool, T. B.; Adjari, A. Propulsion of a molecular machine by asymmetric distribution of reaction products. *Phys. Rev. Lett.* **2005**, *94*, 220801, 1−4.
(14) Kirchhoff, R.; Lowen H, H. T-structured fluid and jamming in driven Brownian rotators. *Europhys. Lett.* **2005**, *69*, 291−297.
(15) Edwards, D. A.; Brenner, H.; Wasan, D. T. Interfacial transport processes and rheology. Butterworth-Heinemann Series in Chemical Engineering; Butterworth-Heinemann: Oxford, 1991.
(16) Ghaskadvi, R. S.; M. Dennin Effect of subphase Ca++ ions on the viscoelastic properties of Langmuir monolayers. *J. Chem. Phys.* **1999**, *111*, 3675−3678.
(17) Ghaskadvi, R. S.; Dennin, M. Alternate measurement of the viscosity peak in heneicosanoic acid monolayers. *Langmuir* **2000**, *16*, 10553−10555.
(18) Ignes-Mullol, J.; Schwartz, D. K. Shear-induced molecular precession in a hexatic Langmuir monolayer. *Nature* **2001**, *410*, 348−351.
(19) Ivanova, A. T.; Ignes-Mullol, J.; Schwartz, D. K. Microrheology of a sheared Langmuir monolayer: Elastic recovery and interdomain slippage. *Langmuir* **2001**, *17*, 3406−3411.
(20) Bantchev, G. B.; Schwartz, D. K. Surface shear rheology of beta-casein layers at the air/solution interface: Formation of a two-dimensional physical gel. *Langmuir* **2003**, *19*, 2673−2682.
(21) Twardos, M.; Dennin, M. Comparison of steady-state shear viscosity and complex shear modulus in Langmuir monolayers. *Langmuir* **2003**, *19*, 3542−3544.

(22) Klingler, J. F.; McConnell, H. Brownian-motion and fluid-mechanis of lipid monolayer domains. *J. Phys. Chem*. **1993**, *97*, 6096−6100.
(23) Schwartz, D.; Knobler, C. M.; Bruinsma, R. Direct observation of Langmuir monolayer flow-through a channel. *Phys. Rev. Lett*. **1994**, *73*, 2841−2844.
(24) Stone, H. A.; Ajdari, A. Hydrodynamics of particles embedded in a flat surfactant layer overlying a subphase of finite depth. *J. Fluid. Mech*. **1998**, *369*, 151−173.
(25) Barentin, C.; Ybert, C.; DiMeglio, J. M.; Joanny, J. F. Surface shear viscosity of Gibbs and Langmuir monolayers. *J. Fluid Mech*. **1999**, *397*, 331−349.
(26) Steffen, P. Heinig, P.; Wurlitzer, S.; Khattari, Z.; Th. Fischer, M. The translational and rotational drag on Langmuir monolayer domains. *J. Chem. Phys*. **2001**, *115*, 994−997.
(27) Wurlitzer, S.; Schmiedel, H.; Fischer, Th. M. Electrophoretic relaxation dynamics of domains in Langmuir monolayers. *Langmuir* **2002**, *18*, 4393−4400.
(28) Sickert, M.; Rondelez, F. Shear Viscosity of Langmuir Monolayers in the Low-Density Limit. *Phys. Rev. Lett*. **2003**, *90*, 126104.
(29) Fischer, Th. M. Comment on: Shear Viscosity of Langmuir Monolayers in the Low-Density Limit. *Phys. Rev. Lett*. **2004**, *92*, 139603.
(30) Sickert, M.; Rondelez, F. Sickert and Rondelez Reply. *Phys. Rev. Lett*. **2004**, *92*, 139604.
(31) Saffman, P. G.; Delbrück, M. Brownian-motion in biological-membranes. *Proc. Natl. Acad. Sci. U.S.A.* **1975**, *72*, 3111−3113.
(32) The 2d viscosity like the 2d pressure have units that differ from their 3d analogues. Surface viscosity is measured in N s/m or surface poise (1 sP = 1 g/s).
(33) Hughes, B. D.; Pailthorpe, B. A.; White, L. R. The translational and rotational drag on a cylinder moving in a membrane. *J. Fluid Mech*. **1981**, *110*, 349−372.
(34) Fischer, Th. M.; Heinig, P.; Dhar, P. The viscous drag of spheres and filaments moving in membranes or monolayers. Submitted for publication in *J. Fluid Mech*.
(35) Stone, H. A. Mobility of membrane-trapped particles: Protrusion into the surrounding fluid. Submitted for publication in *J. Fluid Mech*.
(36) Th. Fischer, M. The drag on needles moving in a Langmuir monolayer. *J. Fluid. Mech*. **2004**, *498* 123−137.
(37) Shlesinger, M. F.; West, B. J.; Klafter, J. Levy dynamics of enhanced diffusion: application to turbulence. *Phys. Rev. Lett*. **1987**, *58*, 1100.
(38) Burgers, J. M. In *Second report on viscosity and plasticity*; North-Holland Publ. Co.: Amsterdam, 1938.
(39) Bouchama, F.; di Meglio, J. M. Two-dimensional rheology of soap films. *J. Phys.*: *Condens. Matter* **1996**, *8*, 9525−9529.
(40) Khattari, Z.; Ruschel, Y.; Wen, H. Z.; Fischer, A.; Fischer, Th. M. Compactification of a myelin mimetic Langmuir Monolayer upon adsorption and unfolding of myelin basic protein. *J. Phys. Chem. B* **2005**, *109*, 3402−3407.
(41) Anderson, J. L. Colloidal transport by interfacial forces. *Annu. Rev. Fluid Mech*. **1989**, *21*, 61.
(42) Kline, T. R.; Paxton, W. F.; Wang, Y.; Velegol, D.; Mallouk, T. E.; Sen, A. Catalytic Micropumps: Microscopic Convective Fluid Flow and Pattern Formation. *J. Am. Chem. Soc*. **2005** (published ASAP).

NL052027S